RSC Advances

PAPER

View Article Online
View Journal | View Issue

Cite this: *RSC Adv.*, 2026, **16**, 17972

Photoredox-enabled late-stage functionalization of pyrrolidines in batch and flow: rapid access to benzothiazole hybrids as a new class of cholinesterase inhibitors

A. Filipović,[a] M. Vučkovski,[b] D. Mićović,[b] A. M. Bondžić [b] and B. P. Bondžić *[a]

A visible-light-driven photoredox protocol for the α-amino C(sp^3)–H heteroarylation of *N*-aryl pyrrolidines and piperidines with 2-chlorobenzothiazole derivatives in batch and in flow conditions is developed. The transformation proceeds under mild conditions using an iridium photocatalyst in the presence of water, providing efficient access to benzothiazole-amine hybrid structures. After initial optimization in batch, the reaction was successfully translated to microfluidic flow, where enhanced light utilization and improved mass and heat transfer enabled higher productivity and superior energy efficiency compared to batch procedures. The scope of the method encompasses a broad range of substituted *N*-aryl pyrrolidines and benzothiazoles, affording the desired products in generally good to excellent yields. In total, a diverse library of benzothiazole–pyrrolidine and –piperidine derivatives was synthesized. The obtained compounds were evaluated for their physicochemical properties and biological activity against acetyl- and butyrylcholinesterase enzymes. Several derivatives exhibited inhibition of these enzymes in the micromolar range, with few molecules showing selectivity towards butyrylcholinesterase. *In silico* ADME analysis indicated favorable lipophilicity and predicted blood–brain barrier permeability. The synergistic combination of photoredox catalysis and microflow technology allowed an efficient and sustainable approach to the late-stage functionalization of biologically relevant amines and the rapid generation of a neuroactive small-molecule library.

Received 5th February 2026
Accepted 27th March 2026

DOI: 10.1039/d6ra01041e

rsc.li/rsc-advances

1. Introduction

Over the past decade photoredox catalysis has become one of the fastest growing areas in organic chemistry. Using light as a readily available reagent, coupled with transition metal or organic photocatalysts led to the development of a plethora of light driven processes.[1–5] A significant area of research in the photoredox catalysis field is late stage functionalizations,[6–9] particularly C–H functionalizations,[10,11] a promising approach in the synthesis of new pharmaceuticals. In that regard α-amino radical formation *via* visible light promoted single electron oxidation of amines and further functionalization of this open-shell species is an important tool for the synthesis of α-functionalized amines, promising structures with a potential wide field of biological activities. In the first example of a photoredox catalyzed α-amino C–H arylation reaction of aliphatic amines with electron deficient heteroarenes, only two examples of reaction with benzothiazole and benzoxazole were presented.[12] This study was extended showcasing the direct α-heteroarylation of tertiary amines with a variety of five- and six-membered chloro-heteroarenes.[13] In addition, C–H functionalization of tertiary aliphatic amines with a number of 2-chloroazole derivatives catalyzed by tris-*fac*-Ir(ppy)$_3$ under the blue light irradiation was reported.[14] Transition-metal-free reaction of 2-chlorobenzazoles with aliphatic carbamates, alcohols, and ethers was achieved using benzophenone as a photocatalyst under the UV-A irradiation at ambient temperature.[15] Dual-catalytic platform for the cross dehydrogenative-coupling between (benzo-)thiazoles and amines combined low loadings of an iridium photoredox catalyst and a cobaloxime catalyst under blue light irradiation.[16]

Functionalized pyrrolidines and piperidines are present in the nature in the form of bioactive alkaloids and are extensively used by pharma industry and academic groups in the pursuit for biologically active molecules. Piperidine and pyrrolidine in particular are very often found in approved as well as in the investigational and experimental drugs.[17] Pyrrolidine is the most commonly found non-aromatic nitrogen heterocycle in the marketed drugs.[18] They are present as a core structure as well as a pharmacophore used to impose certain desired properties upon larger molecule. Among the well-known drugs with

[a]*University of Belgrade-Institute of Chemistry, Technology and Metallurgy, National Institute of the Republic of Serbia, Njegoševa 12, 11000 Belgrade, Serbia. E-mail: bojan.bondzic@ihtm.bg.ac.rs*

[b]*Vinča Institute of Nuclear Sciences, National Institute of the Republic of Serbia, University of Belgrade, P.O. Box 522, 11000 Belgrade, Serbia*

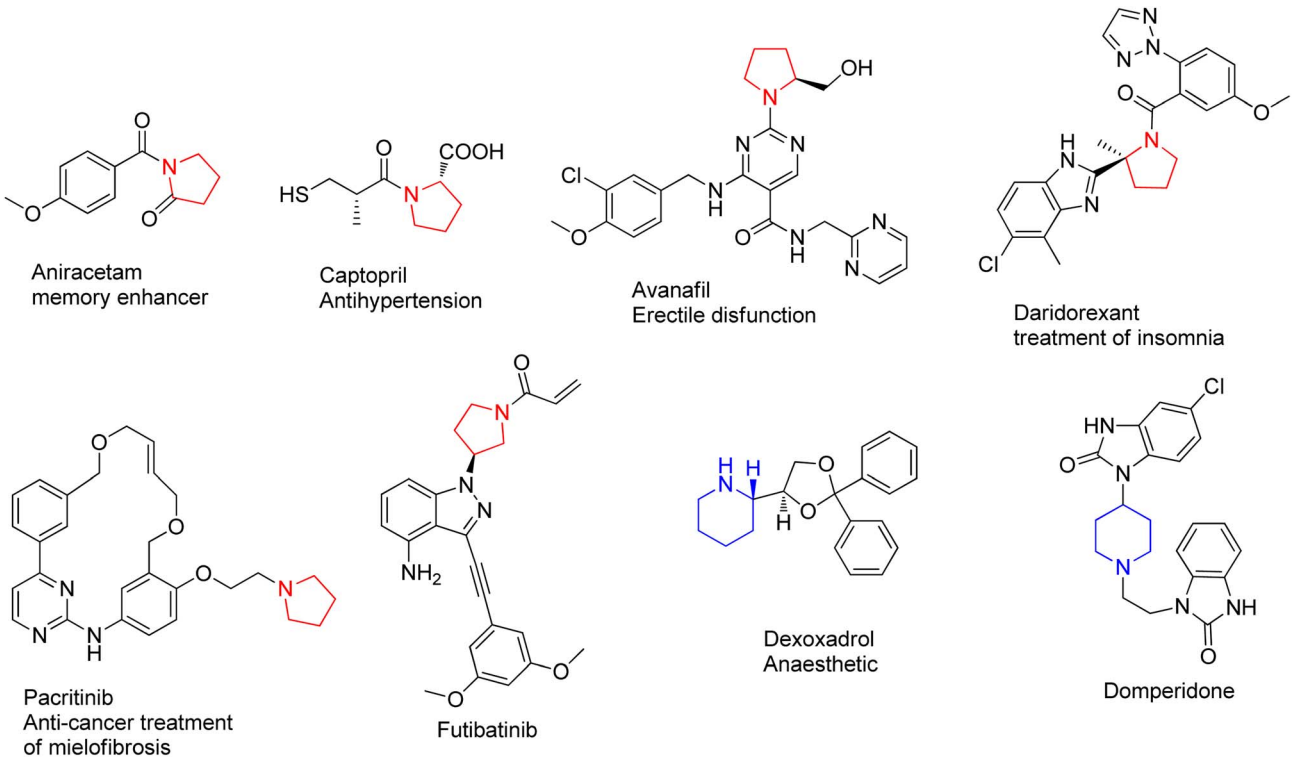

Fig. 1 Some of the commercially available drugs containing pyrrolidine and piperidine scaffold.

a pyrrolidine or piperidine ring, some of the very recently approved molecules (2022) containing pyrrolidine ring include daridorexant (insomnia), pacritinib (JAK-2 inhibitor), and futibatinib 14 (FGFR-4 inhibitor) (Fig. 1).[19] Additionally, pyrrolidine and derivatives are very often used as ligands in transition metal catalysis and as catalysts in organo-catalysis.[20–22]

On the other hand, benzothiazoles represent prominent structural motif in a wide range of biologically active molecules and are attractive target structures in medicinal chemistry.[23] Their biological activity is reflected in ability to inhibit various therapeutic targets such as the cyclooxygenase-2 (COX-2), the enzyme linked with inflammation, pain, and fever,[24] the vascular endothelial growth factor receptor-2 (VEGFR-2), the receptor crucial for tumor growth and angiogenesis,[25] the tyrosinase, the enzyme involved in melanin production, with potential for skin-whitening agents and antioxidants.[26] Recently published study also clearly demonstrated the inhibitory potential of benzothiazole derivatives against enzymes involved in the pathogenesis of neurodegenerative diseases, such as the monoamine oxidase B (MAO-B),[27] acetyl- (AChE) and butyrylcholinesterase (BuChE),[28,29] highlighting this scaffold as a potential chromophore in the development of new anti-neurodegenerative drugs. Additionally, there are several notable drugs that incorporate this moiety (Fig. 2).

Functionalization of (benz)azoles was previously achieved with a variety of transition-metal-catalyzed C–C and C–N

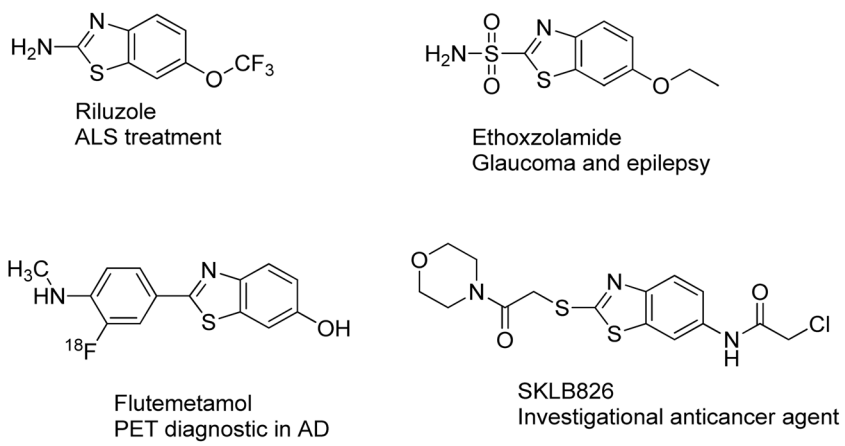

Fig. 2 Drugs and investigational compounds incorporating benzthiazole structures.

coupling reactions using the copper, nickel, or palladium catalysis.[30] In our study we wanted to perform thorough examination of photoredox catalyzed α-amino C(sp^3)–H heteroarylation of *N*-aryl pyrrolidines and piperidines with 2-chlorobenzazole derivatives to obtain number of potentially active molecules against cholinergic enzymes. Various pyrrolidine derivatives have already shown cholinergic activity, such as dispiro–indeno pyrrolidine/pyrrolothiazole–thiochroman hybrids,[31] spirooxindole-pyrrolidine derivatives,[32] or *N*-benzyl-pyrrolidine derivatives.[33]

We expected that merger of these biological active scaffolds, pyrrolidine's ring with benzothiazoles, should provide good starting point for enhancement of biological activity of hybrid compounds as for instance shown in a series of benzimidazole pyrrolidine hybrid molecules that were synthesized by Min *et al.* as inhibitors of poly(ADP-ribose) for treatment of cancer.[34] This endeavor is in line with our recent work in the field of cholinergic enzymes inhibitors as potential Alzheimer's disease therapies.[35–37] In addition, to make the functionalization practical and more efficient we also envisaged use of the microfluidic chemistry methodology as a green and efficient synthetic method.

2. Experimental

2.1. General remarks

All reactions were monitored by thin-layer chromatography using Merck 60 F254 precoated silica gel plates (0.25 mm thickness). Preparative thin layer chromatography was performed using Merck 60 F254 silica gel purchased from Merck KGA. Column chromatography was carried out on silica gel (12–26, ICN Biomedicals) using petrol ether/ethyl acetate as eluents. ^{1}H-NMR and ^{13}C-NMR spectra were measured on a Bruker Ultrashield Advance III spectrometer (^{1}H at 500 MHz, ^{13}C at 125 MHz) and Varian 400 sprectrometer (^{1}H at 400 MHz, ^{13}C at 100 MHz) using $CDCl_3$ as solvent with TMS as internal standard. Chemical shifts (δ) are given in parts per million (ppm) and coupling constants are given in Hertz (Hz).The proton spectra are reported as follows δ per ppm (multiplicity, coupling constant J Hz^{-1}, number of protons). High-resolution mass spectral analyses (HRMS) were carried out using Bruker ESI-TOF MS. IR spectra were measured on a PerkineElmer FT-IR 1725X spectrophotometer using ATR technique. The peak intensities are defined as very strong (*vs.*), strong (s), middle (m) or weak (w).

2.2. Materials and methods

2.2.1 Chemicals. Dimethyl sulfoxide (DMSO), ethanol, methanol acetylcholinesterase (AChE), butyrylcholinesterase (BuChE), acetylthiocholine iodide (AChI), butyrylthiocholine iodide (BuChI), 5,5′-dithiobis (2-nitrobenzoic acid) (DTNB) and sodium dodecyl sulfate (SDS) were obtained from Sigma-Aldrich, Germany.

2.2.2 General procedure for the photoredox catalyzed functionalization of *N*-aryl amines in batch. *N*-aryl amine (2 equiv., 0.5 mmol), benzothiazole (1 equiv., 0.25 mmol), $[Ir(dtbbpy)(ppy)_2]PF_6$ cat. (0.0025 mmol, 1 mol%), sodium acetate (2 equiv., 0.5 mmol) were added in a mixture of dimethylacetamide (1 mL) and H_2O (65 equiv., 0.3 mL) in a flame dried glass vial. The solution was sparged with argon for 15 minutes to remove oxygen. The mixture was stirred for 24 hours under 24 W blue, light emitting diodes (LEDs) irradiation in a custom-made photo reactor. Reaction progress was followed with thin layer chromatography (TLC). Upon completion of the reaction, reaction mixture was diluted with ethyl acetate (20 mL) and water (30 mL). This solution was transferred to separatory funnel and extracted with 30 mL brine (4×). Organic layer was dried with anhydrous $MgSO_4$, filtered and solvent was evaporated under reduced pressure on the vacuum evaporator. Purification was performed using SiO_2 column chromatography or preparative thin layer chromatography (PTLC) using petrol ether/ethyl acetate or toluene/ethyl acetate mixtures as an eluent.

2.2.3 General procedure for the photoredox catalyzed functionalization of *N*-aryl amines in flow. *N*-aryl amine (2 equiv., 0.5 mmol), benzothiazole (1 equiv., 0.25 mmol), $[Ir(dtbbpy)(ppy)_2]PF_6$ cat. (0.0025 mmol, 1 mol%), sodium acetate (2 equiv., 0.5 mmol) were added in a mixture of dimethylacetamide (1 mL) and H_2O (65 equiv., 0.3 mL) in a flame dried glass vial. The solution was sparged with argon for 15 minutes to remove oxygen. The mixture was transferred to 2 mL syringe, placed on a syringe pump and connected to FEP reactor. Reaction mixture was pumped at designated flow rate under 24 W blue LED irradiation in a custom-made photo reactor. After all the solution was pumped through the reactor and collected in recipient flask, reaction mixture was diluted with ethyl acetate (20 mL) and water (30 mL). This solution was transferred to separatory funnel and extracted with 30 mL brine (4×). Organic layer was dried with anhydrous $MgSO_4$, filtered and solvent was evaporated under reduced pressure on the vacuum evaporator. Purification was performed using SiO_2 column chromatography or preparative thin layer chromatography (PTLC) using petrol ether/ethyl acetate or toluene/ethyl acetate mixtures as an eluent.

2.2.4 Measurement of AChE and BuChE activity. The ability of compounds to inhibit AChE and BuChE activity was assessed according to Ellman's method, using AChI and BuChI as enzyme substrates and DTNB as the chromogenic reagent. Stock solutions of AChE and BuChE were diluted with 20 mM TRIS and deionized water, respectively, to achieve an enzyme activity of 1 unit per mL. AChI and BuChI solutions (0.075 M) were prepared in deionized water, while a 0.01 M DTNB solution was made with 0.1 M phosphate buffer (pH 7) containing 0.15% (w/v) sodium bicarbonate. The compounds under investigation were prepared daily as 10 mM stock solutions by dissolving them in DMSO, with further dilutions also done in DMSO. Enzyme assays were set up as follows: 0.1 M phosphate buffer (pH 8.0), 20 μM DTNB, the test compound at a desired concentration (1×10^{-5} M for the screening test or varying concentrations for IC_{50} determination), and 0.0285 U mL^{-1} AChE (or BuChE) were preincubated at 37 °C for 30 minutes. The enzyme reaction was initiated by adding 10 μl (7.5 mM) of AChI (or BuChI), and the assay mixture was incubated at 37 °C for 6 minutes. The reaction was stopped by adding 0.1 M SDS.

Absorbance was measured at 412 nm using a Lambda 35, PerkinElmer spectrophotometer. Quartz cuvettes with an optical path length of 10 mm were used for measurements. Assay containing all components except the enzyme (blank), was used to account for non-enzymatic reactions, while a control solution lacked the inhibitor. All experiments were performed in triplicate, and the results are presented as the mean percentage of enzyme activity relative to the control. IC_{50} values were calculated from log concentration-inhibition curves using Origin 9 on Microsoft Windows.

2.2.5 Lipophilicity and BBB permeability prediction. Lipophilicity and BBB permeability of selected benzothiazole derivates were predicted *in silico* using free software SwissADME.[38]

3. Results and discussion

3.1. Synthesis of benzothiazole–pyrrolidine derivatives in batch

We started our study by firstly optimizing reaction conditions in batch using *N*-phenyl pyrrolidine and 2-chlorobenzthiazole as model reactants, using different photocatalysts in the presence of DMA as a solvent and various amounts of water as a co-solvent. Small amounts of water have already been shown to be beneficial for this reaction and NaOAc has been established as the base of choice for this type of reaction.[12,13] Solubility of an inorganic base is a very important factor when establishing synthetic protocol that would also be viable under microfluidic conditions. Solids could precipitate leading to unrepeatable results or reaction interruption upon clogging of channels. In that regard we examined the effect of amount water on the reaction outcome. In the presence of 1 mol% $[Ir(dtbbpy)(ppy)_2]PF_6$ as a catalyst and 2 equivalents of NaOAc as a base while increasing amounts of water from 0 to 65 equivalents (Table 1, entries 1–4) we observed an increase in the reaction yield. Best results were obtained with 65 equivalents of water in which case reaction mixture was homogeneous. Further increase up to 185 equivalents of water led to deteriorating yield and only 15% of desired compound was isolated (Table 1, entry 5). Other Ir catalysts and organic catalysts such as TPP and acridinium type catalyst did not give better yields compared to initial Ir catalyst (Table 1 entries 6–10). After reaction conditions were optimized series of *N*-aryl substituted pyrrolidines were reacted with various 2-chloro benzthiazoles in order to establish the scope of the reaction.

In all cases better yields were obtained with unsubstituted **2a** or Cl-substituted **2c**. Methoxy substituted benzothiazole **2d** in general gave bit lower yields of desired product in the most of the cases while fluorine substituted **2b** gave very good yields in general a bit lower than Cl substituted **2c** probably due to the pronounced mesomeric effect of fluorine in **2b**. This behavior can be explained by the fact that according to previously established mechanism reaction most likely proceeds through addition of α-amino radical to heteroarene, in which case electron density at heteroarene's C-2 plays a very significant role. Various substituents at the aryl part of pyrrolidine are tolerated in this reaction, unsubstituted (Table 2, entries 1–4) or Me substituted substrates at R^2 (Table 2, entries 5–8), R^2 and R^3 (Table 2, entries 13–16) and at R^3 (Table 2, entries 17–20), react efficiently giving products in good to excellent yields. Electron donating OMe at position R^2 (Table 2, entries 21–24) and at R^1–R^3 (Table 2, entries 29–31) also gave very good yields of desired products, reaction is efficient and bit faster judging by the TLC analysis which might be in line with increased electron density of nucleophilic α-amino radical in this case. Electron

Table 1 Optimization of photoredox α-heteroarylation of *N*-aryl pyrrolidines with 2-chloro benzthiazoles

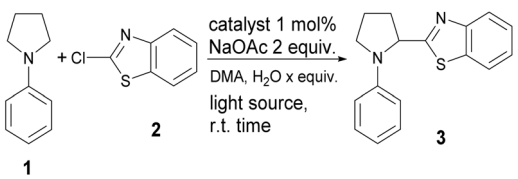

Entry[a]	Photocatalyst (*x* mol%)	H_2O (equiv.)	Light	Yield (%)[b]
1	$[Ir(dtbbpy)(ppy)_2]PF_6$ (1 mol%)	0	Blue LED	51
2	$[Ir(dtbbpy)(ppy)_2]PF_6$ (1 mol%)	10	Blue LED	72
3	$[Ir(dtbbpy)(ppy)_2]PF_6$ (1 mol%)	25	Blue LED	76
4	$[Ir(dtbbpy)(ppy)_2]PF_6$ (1 mol%)	65	Blue LED	87
5	$[Ir(dtbbpy)(ppy)_2]PF_6$ (1 mol%)	185	Blue LED	35
6	$Ir[dF(CF_3)ppy]_2(dtbpy)PF_6$ (1 mol%)	65	Blue LED	77
7	$Ir(ppy)_3$ (1mol%)	65	Blue LED	60
8	TPP (5 mol%)	65	Blue LED	10
9	9-Mesityl-3,6-di-*tert*-butyl-10-phenylacridinium tetrafluoroborate (5 mol%)	25	Blue LED	n.r.
10	9-Mesityl-10-methylacridinium perchlorate (5 mol%)	25	Blue LED	n.r.

[a] Reaction conditions: phenylpyrrolidine (0.5 mmol, 2 equiv.), Ir cat. (0.0025 mmol, 1 mol%), NaOAc (0.5 mmol, 2 equiv.) and benzothiazole (0.25 mmol, 1 equiv.) were added to DMA (1 mL) and H_2O (see table) mixture, and sparged with argon for 15 minutes to remove oxygen. Solution was irradiated with 24 W blue LED and stirred for designated period of time. [b] Isolated yield after column chromatography.

Table 2 Photoredox α-heteroarylation of *N*-aryl pyrrolidines with 2-chloro benzothiazoles

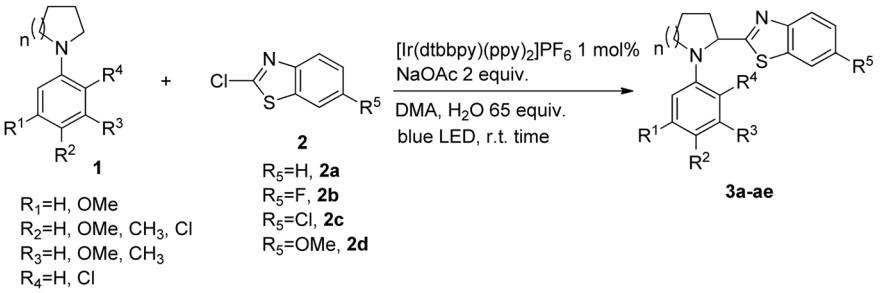

Entry[a]	Compound	Structure						Yield[b] (%)
		n	R1	R2	R3	R4	R5	
1	**3a**	1	H	H	H	H	H	87
2	**3b**	1	H	H	H	H	F	61
3	**3c**	1	H	H	H	H	Cl	69
4	**3d**	1	H	H	H	H	OCH_3	75
5	**3e**	1	H	CH_3	H	H	H	75
6	**3f**	1	H	CH_3	H	H	F	66
7	**3g**	1	H	CH_3	H	H	Cl	70
8	**3h**	1	H	CH_3	H	H	OCH_3	82
9	**3i**	1	H	H	CH_3	H	H	77
10	**3j**	1	H	H	CH_3	H	F	78
11	**3k**	1	H	H	CH_3	H	Cl	81
12	**3l**	1	H	H	CH_3	H	OCH_3	82
13	**3m**	1	H	CH_3	CH_3	H	H	67
14	**3n**	1	H	CH_3	CH_3	H	F	73
15	**3o**	1	H	CH_3	CH_3	H	Cl	89
16	**3p**	1	H	CH_3	CH_3	H	OCH_3	79
17	**3q**	1	H	OCH_3	H	H	H	88
18	**3r**	1	H	OCH_3	H	H	F	77
19	**3s**	1	H	OCH_3	H	H	Cl	76
20	**3t**	1	H	OCH_3	H	H	OCH_3	81
21	**3u**	1	OCH_3	OCH_3	OCH_3	H	H	84
22	**3v**	1	OCH_3	OCH_3	OCH_3	H	F	74
23	**3w**	1	OCH_3	OCH_3	OCH_3	H	Cl	75
24	**3x**	1	H	Cl	H	H	H	79
25	**3y**	1	H	Cl	H	H	F	63
26	**3z**	1	H	Cl	H	H	Cl	69
27	**3aa**	1	H	Cl	H	H	OCH_3	72
28	**3ab**	1	H	H	H	Cl	H	75
29	**3ac**	1	H	H	H	Cl	F	80
30	**3ad**	1	H	H	H	Cl	Cl	79
31	**3ae**	1	H	H	H	Cl	OCH_3	70
32	**4a**	2	H	H	H	H	H	62
33	**4b**	2	H	H	H	H	F	64
34	**4c**	2	H	H	H	H	Cl	56
35	**4d**	2	H	H	H	H	OMe	76

[a] Reaction conditions: phenylpyrrolidine (0.5 mmol, 2 equiv.), Ir cat. (0.0025 mmol, 1 mol%) sodium acetate (0.5 mmol, 2 equiv.) and benzothiazole (0.25 mmol, 1 equiv.) were added to solvent DMA (1 mL) and water (16.25 mmol, 65 equiv., 0.3 mL) mixture and sparged with argon for 15 minutes to remove oxygen. Solution was irradiated with 24 W blue LED and stirred for designated period of time. [b] Isolated yield after column chromatography.

withdrawing Cl substituent at R^4 (Table 2, entries 9–12) or at R^2 (Table 2, entries 25–28) also gave very good yields of desired products. In addition, *N*-aryl substituted piperidines also react with 2-chloro benzthiazoles in the similar manner to pyrrolidines under optimized reaction conditions using 1 mol% $[Ir(dtbbpy)(ppy)_2]PF_6$ as a catalyst and DMA/water as a solvent under 24W LED irradiation. In general, lower yields compared to reactions with pyrrolidines are obtained. Reaction proceeds with benzthiazoles **2a–d** under optimized conditions to give desired products in 56–76% yield (Table 2, entries 32–35). In total, 35 compounds with different substitution pattern were synthesized. Wide array of available substituents at the aryl part of the molecule is accompanied by the various substituents at the benzothiazole part of the hybrid molecule.

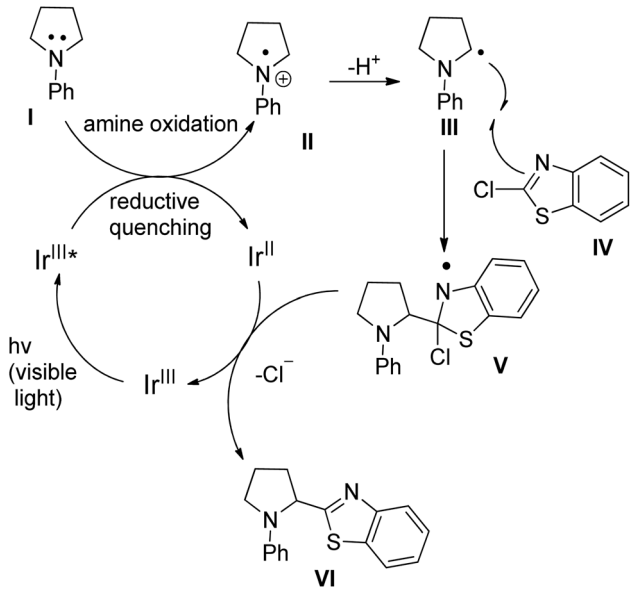

Scheme 1 Plausible reaction mechanism *via* homolytic aromatic substitution.

Plausible reaction mechanism of α-amino C(sp^3)–H heteroarylation of *N*-aryl pyrrolidines has been previously proposed and involves single-electron oxidation of amine **I** followed by deprotonation to give α-amino radical **III** (Scheme 1).[13] Radical **III** reacts with neutral chloro-heteroarene **IV** *via* a homolytic aromatic substitution pathway giving intermediate **V**. Reduction of this intermediate with Ir^{II} followed by release of chlorine anion provides final product **VI**.

3.2. Synthesis of benzothiazole–pyrrolidine derivatives in microfluidic reactor

Next, we turned our attention to transferring our optimized reactions to microfluidic reactors. In general, it is very often possible to apply optimized batch conditions to microflow directly, with required optimization of the residence time and light intensity. Choice of microreactor type is important in regard to applied reaction conditions such as oxygen sensitivity, reactor transparency for various wavelengths, heat and mass transfer capability.

Application of flow chemistry in the synthesis of valuable organic molecules is a well-established method.[39–42] Lately, visible light promoted photoredox catalysis is one of the areas in which microfluidic chemistry has shown great potential for application and improvement of batch processes.[43–47] High surface-area-to-volume ratios characteristic of these systems

Table 3 Optimization of reaction conditions in microfluidic reactor

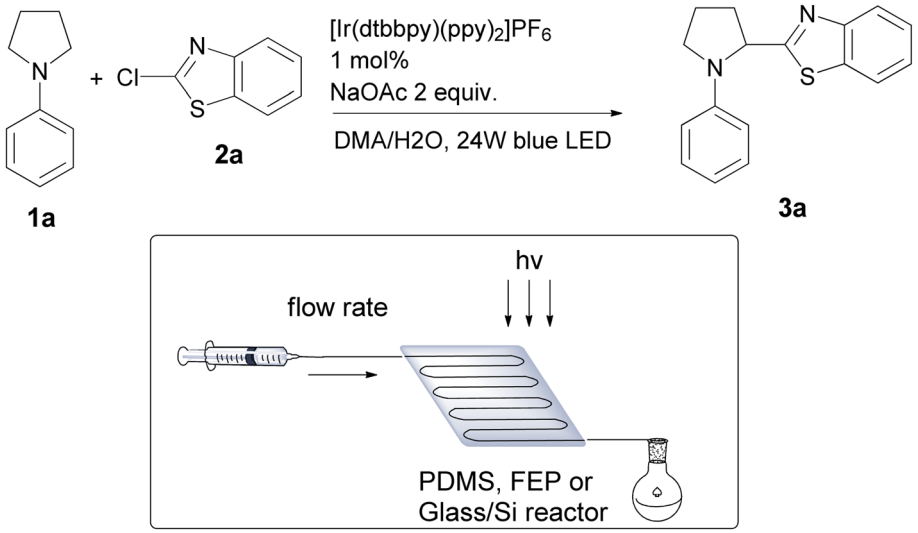

Entry[a]	Reactor type	Reactor volume (cm^3)	Residence time (h)	Yield[b] (%)	% W^{-1} h^{-1}	STY[c] (mmol l^{-1} h^{-1})	Productivity[c] (mg h^{-1})
1	Batch	1.5	24	87	0.15	7.2	2.54
2	FEP	0.5	4	64	0.66	30.8	2.80
3	PDMS	0.5	4	43	0.45	20.4	1.88
4	Glass/Si	0.025	4	21	0.22	10.8	0.048
5	FEP	0.5	6	92	0.64	29.4	2.69

[a] Reaction conditions: *N*-phenyl pyrrolidine (0.5 mmol, 2 equiv.), Ir cat. (0.0025 mmol, 1 mol%) sodium acetate (0.5 mmol, 2 equiv.) and benzothiazole (0.25 mmol, 1 equiv.) were added to DMA (1 mL) and water (16.25 mmol, 65 equiv., 0.3 mL) mixture and sparged with argon for 15 minutes to remove oxygen. Solution was pumped through the microreactor using syringe pump and irradiated with 24 W blue LED for designated period of time. [b] Isolated yield after column chromatography. [c] Space-time yield (STY) and productivity are calculated according to formulae shown in the SI.

allow improved light utilization and better heat and mass transfer effects in photochemical transformations. Our group recently used readily available Ru catalyst and polydimethyl siloxane (PDMS) matrices in the microfluidic functionalization of tetrahydroisoquinolines (THIQs) using Manich, Strecker or alkynilation protocols.[48] In addition, we showcased one of the first examples of formation and functionalization of THIQ derived α-aminoradicals under microflow conditions.[49]

We started by testing PDMS, Glass/Silicon and fluorinated ethylene propylene (FEP) polymer tube reactors (Table 3). Among tested reactors FEP tube reactor gave the best yields of 64% of the desired product after 4 h or residence time (Table 3, entry 2). PDMS and Glass/Si reactor gave lower yields of desired product most probably due to oxygen porosity in case of PDMS and much thinner channels and occasional clogging in Glass/Si reactor leading to uneven reaction flow and pressure drops. After 4 h of residence time there is still unreacted starting material in FEP reactor, increase of the residence time to 6 h led to full conversion of starting material and 92% yield of the desired product (Table 3, entry 5).

Surface to volume ratio for PDMS, Glass/Si and FEP microreactor are similar, around 5000 m^2 m^{-3} which is in the range for a microreactor device according to De Santis.[50] Energy efficiency of the microreactors was also calculated and data are given in the Table 3. The energy efficiency of different light sources and reactors can be assessed through parameter defined as the ratio of percent product yield per W h^{-1} (Table 3).[51] The best values of 0.64 of energy efficiency of light sources and the energy efficiency of the reactor are obtained for the FEP microreactor with a residence time of 6 h and LED irradiation of 24 W (Table 3, entry 5). It can be concluded that FAP microreactor has the best utilization of light and is the most energy efficient compared to two other reactors.

Besides product yield and energy efficiency, essential metrics for evaluating reaction performance in batch and microflow conditions are space-time yield (STY) and productivity. These metrics define the efficiency of the reactor and enable a comparison of the different reactors.[52] STY is defined as a measure of reaction effectiveness quantified through the product mass obtained for a certain time in a certain reactor volume. The results for these parameters regarding applied microreactors in our

Table 4 Photoredox α-heteroarylation of *N*-aryl amines under microfluidic conditions

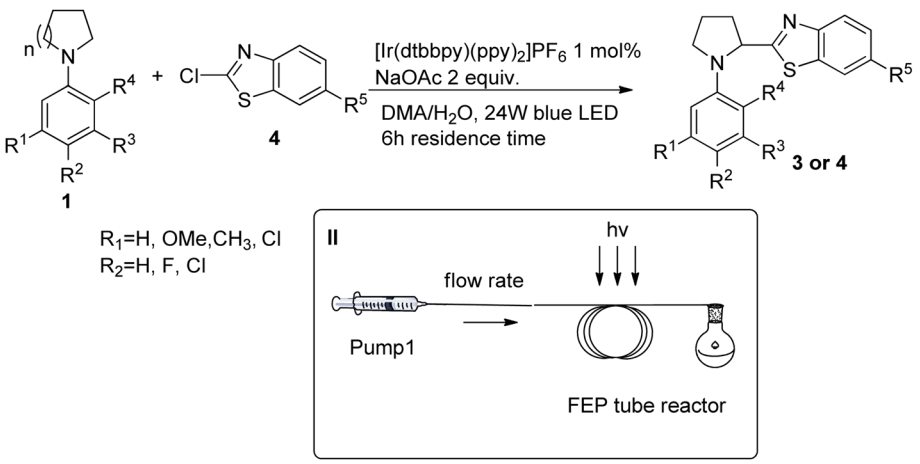

Entry[a]	Compound	*n*	R1	R2	R3	R4	R5	Yield[b] (%)	STY[c] (mmol l^{-1} h^{-1})	Productivity[c] (mg h^{-1})
1	**3a**	1	H	H	H	H	H	92	29.4	2.69
2	**3b**	1	H	H	H	H	F	81	25.8	2.52
3	**3c**	1	H	H	H	H	Cl	87	27.6	2.85
4	**3e**	1	Me	H	H	H	H	85	27.1	2.60
5	**3g**	1	H	Me	H	H	Cl	89	28.2	3.05
6	**3o**	1	H	Me	Me	H	Cl	93	30.1	3.32
7	**3u**	1	OMe	OMe	OMe	H	H	91	29.4	3.51
8	**3y**	1	Cl	H	H	H	F	85	27.1	2.95
9	**3z**	1	Cl	H	H	H	Cl	88	28.2	3.20
10	**3aa**	1	Cl	H	H	H	OMe	92	29.4	3.31
11	**3ab**	1	H	H	H	Cl	H	84	27.0	2.75
12	**4a**	2	H	H	H	H	H	79	25.2	2.42

[a] Reaction conditions: *N*-phenyl pyrrolidine or *N*-phenyl piperidine (0.5 mmol, 2 equiv.), Ir cat. (0.0025 mmol, 1 mol%) sodium acetate (0.5 mmol, 2 equiv.) and benzothiazole (0.25 mmol, 1 equiv.) were added to DMA (1 mL) and water (16.25 mmol, 65 equiv., 0.3 mL) mixture and sparged with argon for 15 minutes to remove oxygen. Solution was pumped through the microreactor using syringe pump and irradiated with 24 W blue LED for designated period of time. [b] Isolated yield after column chromatography. [c] Space-time yield (STY) and productivity are calculated according to formulae shown in the SI.

process are summarized in Table 3. As can be seen, STY is 2–3 times higher in PDMS and FEP microreactor compared to batch system (Table 3, entries 2, 3 and 5). The glass/silicon microreactor (Table 3, entry 4) has STY value just slightly higher than the batch most probably due to reaction clogging and uneven flow in the very narrow channels. These results are in accordance with previous reports where STY is 3–4 times higher in microfluidic devices *vs.* batch.[53,54] The best productivity was achieved in FEP microreactor, with a residence time of 4 h (Table 3, entry 2).

Upon reaction conditions optimization under microfluidic conditions generality of the setup was confirmed with several examples (Table 4). In al tested cases better yields were obtained compared to batch conditions. Reactions were run with 6 h residence time irradiated with 24 W blue LEDs.

3.3. Assessment of log *P*, blood–brain permeability and the biological activity of the synthesized benzothiazole derivatives

In the early stages of drug discovery and development, particularly for compounds intended to treat neurological disorders,

Table 5 The inhibition properties of synthesized benzothiazole derivatives, **3a–4d** towards eeAChE and eqBuChE

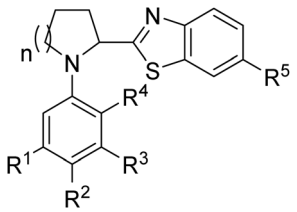

	Structure						Swiss ADME		IC_{50},[a] (μM)	
Compound	*n*	R1	R2	R3	R4	R5	log *P*	BBB	AChE	BuChE
3a	1	H	H	H	H	H	3.42	Yes	>10	6.17 ± 0.98
3b	1	H	H	H	H	F	3.8	Yes	>10	>10
3c	1	H	H	H	H	Cl	3.92	Yes	>10	2.74 ± 1.09
3d	1	H	H	H	H	OCH_3	3.04	Yes	n.a.	3.83 ± 0.47
3e	1	H	CH_3	H	H	H	3.65	Yes	>10	>10
3f	1	H	CH_3	H	H	F	4.04	Yes	>10	>10
3g	1	H	CH_3	H	H	Cl	4.15	Yes	0.95 ± 0.08	2.96 ± 0.40
3h	1	H	CH_3	H	H	OCH_3	3.27	Yes	>10	>10
3i	1	H	H	CH_3	H	H	3.65	Yes	>10	>10
3j	1	H	H	CH_3	H	F	4.04	Yes	>10	>10
3k	1	H	H	CH_3	H	Cl	4.15	Yes	5.65 ± 0.05	3.96 ± 0.06
3l	1	H	H	CH_3	H	OCH_3	3.27	Yes	>10	>10
3m	1	H	CH_3	CH_3	H	H	3.89	Yes	>10	>10
3n	1	H	CH_3	CH_3	H	F	4.27	Yes	>10	>10
3o	1	H	CH_3	CH_3	H	Cl	4.38	Yes	0.78 ± 0.08	2.72 ± 0.02
3p	1	H	CH_3	CH_3	H	OCH_3	3.50	Yes	>10	>10
3q	1	H	OCH_3	H	H	H	3.04	Yes	n.a.	>10
3r	1	H	OCH_3	H	H	F	3.43	Yes	>10	>10
3s	1	H	OCH_3	H	H	Cl	3.54	Yes	>10	>10
3t	1	H	OCH_3	H	H	OCH_3	2.62	Yes	n.a.	>10
3u	1	OCH_3	OCH_3	OCH_3	H	H	2.36	Yes	>10	>10
3v	1	OCH_3	OCH_3	OCH_3	H	F	2.74	Yes	>10	>10
3w	1	OCH_3	OCH_3	OCH_3	H	Cl	2.85	Yes	>10	>10
3x	1	H	Cl	H	H	H	3.92	Yes	>10	>10
3y	1	H	Cl	H	H	F	4.31	Yes	>10	10
3z	1	H	Cl	H	H	Cl	4.42	Yes	>10	>10
3aa	1	H	Cl	H	H	OCH_3	3.54	Yes	>10	10
3ab	1	H	H	H	Cl	H	3.92	Yes	2.81 ± 0.05	>10
3ac	1	H	H	H	Cl	F	4.31	Yes	10	>10
3ad	1	H	H	H	Cl	Cl	4.42	Yes	>10	>10
3ae	1	H	H	H	Cl	OCH_3	3.54	Yes	10	10
4a	2	H	H	H	H	H	3.65	Yes	>10	>10
4b	2	H	H	H	H	F	4.04	Yes	>10	>10
4c	2	H	H	H	H	Cl	4.15	Yes	>10	8.93 ± 0.05
4d	2	H	H	H	H	OCH_3	3.27	Yes	>10	>10

[a] n.a. – no activity; data given represent mean ± standard error (SE) values of the results from three independent experiments performed in triplicates. Predicted log *P* and BBB permeability for synthesized benzothiazole derivatives obtained using Swiss ADME.

adequate lipophilicity and blood–brain barrier (BBB) permeability represent essential prerequisites. Accordingly, log *P*, as an indicator of compound lipophilicity, together with the BBB permeability of the synthesized compounds, was theoretically assessed using SwissADME software, and the results are summarized in Table 5. All compounds displayed log *P* values within the optimal range and were predicted to cross the BBB,[52,55] suggesting their potential to inhibit cholinesterase enzymes, which are closely associated with Alzheimer's disease. On this basis, the synthesized benzothiazole derivatives were further evaluated for their inhibitory activity against acetyl- and butyrylcholinesterase, and the corresponding results are presented in Table 5. Overall, the compounds predominantly exhibited selectivity toward BuChE, with IC_{50} values in the micromolar range, whereas lower or no inhibitory activity against AChE was generally observed. An exception was found among the chloro-substituted derivatives, which displayed inhibitory activity toward both enzymes and yielded the most potent AChE inhibitor, compound **3o**.

Structure-activity relationship analysis revealed that the presence of chlorine in the benzothiazole moiety significantly influenced biological activity. Specifically, chlorination led to a twofold increase in BuChE inhibitory potency, as observed for compound **3c** compared with its non-chlorinated analogue, compound **3a**. Furthermore, variations in substituents (CH_3, Cl, and OCH_3) on the aryl moiety of the pyrrolidine part of the Cl-substituted derivatives resulted in distinct biological activity profiles. Among these, CH_3 substitution markedly enhanced inhibitory potency and additionally enabled AChE inhibition, yielding compounds with dual inhibitory properties (**3g**, **3k**, and **3o**). Notably, the synergistic effect of two CH_3 groups proved particularly important, resulting in potent inhibition of both enzymes, with IC_{50} values for AChE below 1 μM, as exemplified by compound **3o**. In contrast, the introduction of Cl at the ortho position of the aryl moiety led to selective AChE inhibition without affecting BuChE activity (compound **3ab**).

In contrast to the chlorinated analogues, fluorine substitution in the benzothiazole ring led to a decrease in BuChE inhibitory activity compared with compound **3a**, irrespective of the substituents on the aryl moiety of the pyrrolidine unit. Moreover, no inhibitory activity toward AChE was detected for the fluorinated derivatives in any case. On the other hand, introduction of a methoxy group into the non-substituted compound **3a** resulted in an approximately 1.5-fold increase in BuChE inhibitory potency (IC_{50} = 6.17 μM for **3a** *vs.* 3.83 μM for compound **3d**). However, further structural modification of compound **3d** on the aryl moiety of the pyrrolidine part did not yield biologically active derivatives.

Evaluation of the biological activity of piperidine-based benzothiazole derivatives against cholinesterase enzymes revealed generally low inhibitory activity, with IC_{50} values higher than 10 μM, except for compound **4c**, which contains a chlorine substituent on the benzothiazole moiety. Comparison of the IC_{50} value of compound **4c** with that of its structural analogue, compound **3c**, suggests that the size of the heterocyclic ring (piperidine *vs.* pyrrolidine) influences inhibitory activity. The pyrrolidine ring, likely due to its conformational properties or smaller dimensions, appears to confer enhanced inhibitory potency.

Taken together, these results indicate that the most biologically active synthesized benzothiazole aryl pyrrolidines were those containing a 6-Cl-substituted benzothiazole core combined with CH_3 groups on the aryl moiety. This highlights the important role of chloride involvement in enzyme-ligand interactions, as well as the significant contribution of methyl substituents to enhanced binding and inhibitory activity.

4. Conclusion

In conclusion, we have developed robust synthetic protocol for the visible light promoted photoredox functionalization of *N*-aryl pyrrolidines and piperidines with benzothiazoles in the presence of water. 35 compounds were synthesized under batch conditions in good yields showing wide applicability of this method. These hybrid molecules were tested in inhibition assays with cholinergic enzymes important in the development of neurological disorders such as Alzheimer's disease and showed low micromolar activities and good potential for further improvement of the inhibition potentials. Several derivatives showed selectivity towards BuChE enzyme. These hybrid molecules represent a new class of neurologicaly active molecules. *In silico* ADME study supports this conclusion since most active molecules are predicted to be able to pass blood–brain barrier which is a prerequisite for molecules intended for use in the treatment of neurological disorders. Furthermore, optimized conditions were transferred to microfluidic conditions allowing access to practical and greener synthetic pathways for the synthesis of our compounds. Good to excellent yields were obtained using FAP tube custom made reactors.

Author contributions

Ana Filipović: investigation, data curation, formal analysis, visualization, Marija Vučkovski: investigation, data curation, formal analysis, visualization, Dunja Mićović: investigation, data curation, formal analysis, visualization, Aleksandra Bondžić: resource, writing – review and editing, methodology, conceptualization, funding acquisition, supervision, resources, Bojan Bondžić: conceptualization, methodology, writing – original draft, writing – review & editing, supervision, project administration, funding acquisition, resources.

Conflicts of interest

The authors declare that they have no known competing financial interests or personal relationships that could have appeared to influence the work reported in this paper.

Data availability

All relevant data supporting this article are included within the manuscript and supplementary information (SI). Supplementary information: detailed experimental procedures and characterization data for the synthesized compounds, including ^1H, ^{13}C NMR and FT-IR spectra. See DOI: https://doi.org/10.1039/d6ra01041e.

Acknowledgements

This research was supported by the Science Fund of the Republic of Serbia, Grant No. 7451, Plasmonic-based light harvesting for photocatalytic microfluidic devices – PlasmaHarvest. In addition, this research has been financially supported by the Ministry of Science, Technological Development, and Innovation of the Republic of Serbia (contract numbers: 451-03-33/2026-03/200017, 451-03-33/2026-03/200026 and 451-03-33/2026-03/200168).

References

1 M. A. Ischay, M. E. Anzovino, J. Du and T. P. Yoon, *J. Am. Chem. Soc.*, 2008, **130**, 12886–12887.
2 D. A. Nicewicz and D. W. C. MacMillan, *Science*, 2008, **322**, 77–80.
3 N. J. W. Straathof, B. J. P. Tegelbeckers, V. Hessel, X. Wang and T. Noël, *Chem. Sci.*, 2014, **5**, 4768–4773.
4 A. Talla, B. Driessen, N. J. W. Straathof, L.-G. Milroy, L. Brunsveld, V. Hessel and T. Noël, *Adv. Synth. Catal.*, 2015, **357**, 2180–2186.
5 M. März, J. Chudoba, M. Kohout and R. Cibulka, *Org. Biomol. Chem.*, 2017, **15**, 1970–1975.
6 G. Laudadio, Y. Deng, K. van der Wal, D. Ravelli, M. Nuño, M. Fagnoni, D. Guthrie, Y. Sun and T. Noël, *Science*, 2020, **369**, 92–96.
7 S. Kamijo, T. Hoshikawa and M. Inoue, *Org. Lett.*, 2011, **13**, 5928–5931.
8 T. Hoshikawa and M. Inoue, *Chem. Sci.*, 2013, **4**, 3118–3123.
9 J. N. Capilato, C. R. Pitts, R. Rowshanpour, T. Dudding and T. Lectka, *J. Org. Chem.*, 2020, **85**, 2855–2864.
10 J. Xie, M. Rudolph, F. Rominger and A. S. K. Hashmi, *Angew. Chem. Int. Ed.*, 2017, **56**, 7266–7270.
11 D. Mazzarella, G. E. M. Crisenza and P. Melchiorre, *J. Am. Chem. Soc.*, 2018, **140**, 8439–8443.
12 A. McNally, C. K. Prier and D. W. C. MacMillan, *Science*, 2011, **334**, 1114.
13 C. K. Prier and D. W. C. MacMillan, *Chem. Sci.*, 2014, **5**, 4173–4178.
14 A. Singh, A. Arora and J. D. Weaver, *Org. Lett.*, 2013, **15**, 5390–5393.
15 A. Lipp, G. Lahm and T. Opatz, *J. Org. Chem.*, 2016, **81**, 4890–4897.
16 E. Bergamaschi, C. Weike, V. J. Mayerhofer, I. Funes-Ardoiz and C. J. Teskey, *Org. Lett.*, 2021, **23**, 5378–5382.
17 C. Bhat and S. G. Tilve, *RSC Adv.*, 2014, **4**, 5405–5452.
18 E. Vitaku, D. T. Smith and J. T. Njardarson, *J. Med. Chem.*, 2014, **57**, 10257–10274.
19 D. B. Tiz, L. Bagnoli, O. Rosati, F. Marini, C. Santi and L. Sancineto, *Pharmaceutics*, 2022, **14**, 2538.
20 P. I. Dalko and L. Moisan, *Angew. Chem., Int. Ed.*, 2004, **43**, 5138–5175.
21 K. Higashiyama, H. Inoue and H. Takahashi, *Tetrahedron*, 1994, **50**, 1083–1092.
22 S. Llopis, T. García, Á. Cantín, A. Velty, U. Díaz and A. Corma, *Catal. Sci. Technol.*, 2018, **8**, 5835–5847.
23 C. S. Demmer and L. Bunch, *Eur. J. Med. Chem.*, 2015, **97**, 778–785.
24 M. Kokane, D. Bhosale, D. Raut, P. Hadimani, A. Narale, S. Chaudhari, P. Choudhari and A. Lawand, *Biochem. Biophys. Res. Commun.*, 2025, **793**, 152998.
25 F. A. A. A. Mohamed, D. Kłopotowska, M. K. Abd El-Gaber, A. S. Aboraia, J. Wietrzyk and A. F. Youssef, *Bioorg. Chem.*, 2025, **166**, 109066.
26 M. Usman, A. Alam, Zainab, M. Khan, A. A. Elhenawy, M. Ayaz, M. M. Alanazi, A. Latif, S. A. A. Shah, M. Ali and M. Ahmad, *J. Mol. Struct.*, 2025, **1319**, 139504.
27 M.-H. Nam, M. Park, H. Park, Y. Kim, S. Yoon, V. S. Sawant, J. W. Choi, J.-H. Park, K. D. Park, S.-J. Min, C. J. Lee and H. Choo, *ACS Chem. Neurosci.*, 2017, **8**, 1519–1529.
28 D. H. Dawood and M. M. Anwar, *Eur. J. Med. Chem.*, 2025, **287**, 117331.
29 R. A. Mohamed-Ezzat and G. H. Elgemeie, *RSC Adv.*, 2025, **15**, 41724–41832.
30 L. Ackermann, S. Barfusser and J. Pospech, *Org. Lett.*, 2010, **12**, 724–727.
31 C. Bharkavi, S. V. Kumar, M. A. Ali, H. Osman, S. Muthusubramanian and S. Perumal, *Bioorg. Med. Chem. Lett.*, 2016, **24**, 5873–5883.
32 Y. Huang, W. Min, Q. W. Wu, J. Sun, D. H. Shi and C. G. Yan, *New J. Chem.*, 2018, **42**, 16211–16216.
33 P. K. Choubey, A. Tripathi, P. Sharma and S. K. Shrivastava, *Bioorg. Med. Chem.*, 2020, **28**, 115721.
34 R. Min, W. Wu, M. Wang, Y. Li, Z. Zhang and L. Chen, *Molecules*, 2019, **24**, 1901.
35 D. Jovanović, A. Filipović, R. Suručić, L. Korićanac, J. Žakula, B. P. Bondžić and A. M. Bondžić, *Int. J. Biol. Macromol.*, 2025, **319**, 145524.
36 M. Vučkovski, A. Filipović, M. Jadranin, L. Korićanac, J. Žakula, B. P. Bondžić and A. M. Bondžić, *Int. J. Mol. Sci.*, 2024, **25**, 13076.
37 D. Jovanović, A. Filipović, G. Janjić, T. Lazarević-Pašti, Z. Džambaski, B. P. Bondžić and A. M. Bondžić, *Int. J. Mol. Sci.*, 2024, **25**, 1033.
38 A. Daina, O. Michielin and V. Zoete, *Sci. Rep.*, 2017, **7**, 42717.
39 K. Geyer, J. D. C. Codée and P. H. Seeberger, *Chem. Eur. J.*, 2006, **12**, 8434–8442.
40 P. Watts and C. Wiles, *Chem. Commun.*, 2007, 443–467.
41 D. Webb and T. F. Jamison, *Chem. Sci.*, 2010, **1**, 675–680.
42 C. Stephenson, T. Yoon and D. W. C. MacMillan, *Visible Light Photocatalysis in Organic Chemistry*, Wiley-VCH, Weinheim, 2018.
43 J. W. Beatty and C. R. J. Stephenson, *J. Am. Chem. Soc.*, 2014, **136**, 10270–10273.
44 Y. Su, N. J. W. Straathof, V. Hessel and T. Noël, *Chem. Eur. J.*, 2014, **20**, 10562–10589.
45 E. M. Schuster and P. Wipf, *Isr. J. Chem.*, 2014, **54**, 361–370.
46 F. Lévesque and P. H. Seeberger, *Org. Lett.*, 2011, **13**, 5008–5011.
47 A. C. Gutierrez and T. F. Jamison, *Org. Lett.*, 2011, **13**, 6414–6417.
48 A. Filipović, Z. Džambaski, D. Vasiljević-Radović and B. P. Bondžić, *Org. Biomol. Chem.*, 2021, **19**, 2668–2675.

49 A. Filipović, Z. Džambaski, A. M. Bondžić and B. P. Bondžić, *Photochem. Photobiol. Sci.*, 2023, **22**, 2259–2270.
50 P. De Santis, L.-E. Meyer and S. Kara, *React. Chem. Eng.*, 2020, **5**, 2155–2184.
51 A. Sugimoto, T. Fukuyama, Y. Sumino, M. Takagi and I. Ryu, *Tetrahedron*, 2009, **65**, 1593–1598.
52 C. A. Hone and C. O. Kappe, *Chem.–Methods*, 2021, **1**, 454–467.
53 O. Shvydkiv, A. Yavorskyy, S. B. Tan, K. Nolan, N. Hoffmann, A. Youssef and M. Oelgemöller, *Photochem. Photobiol. Sci.*, 2011, **10**, 1399–1404.
54 A. Yavorskyy, O. Shvydkiv, K. Nolan, N. Hoffmann and M. Oelgemöller, *Tetrahedron Lett.*, 2011, **52**, 278–280.
55 M. Markowicz-Piasecka, A. Markiewicz, P. Darłak, J. Sikora, S. K. Adla, S. Bagina and K. M. Huttunen, *Neurotherapeutics*, 2022, **19**, 942–976.